IEEE Access
Multidisciplinary | Rapid Review | Open Access Journal

Received May 13, 2021, accepted May 31, 2021, date of publication June 4, 2021, date of current version June 15, 2021.

Digital Object Identifier 10.1109/ACCESS.2021.3086680

Impact of High Switching Speed and High Switching Frequency of Wide-Bandgap Motor Drives on Electric Machines

YIPU XU[1], XIBO YUAN[2], (Senior Member, IEEE), FEI YE[1], ZIHAO WANG[1], YONGLEI ZHANG[1], MOHAMED DIAB[2], (Senior Member, IEEE), AND WENZHI ZHOU[2], (Graduate Student Member, IEEE)

[1]School of Electrical and Power Engineering, China University of Mining and Technology, Xuzhou 221000, China
[2]Department of Electrical and Electronic Engineering, University of Bristol, Bristol BS8 1UB, U.K.

Corresponding author: Xibo Yuan (xibo.yuan@bristol.ac.uk)

ABSTRACT The emergence of fast-switching wide-bandgap (GaN, SiC) power electronics devices has enabled motor drive systems to achieve high efficiency, power density, control bandwidth and high-level of integration. However, the fast-switching speed and high switching frequency result in an increased level of motor overvoltage at both motor terminals and stator neutral. This overvoltage increases the stress across the motor winding insulation and bearings. This paper investigates three types of motor overvoltages, i.e., differential mode (DM) (phase-to-phase) motor terminal overvoltage, common mode (CM) (phase-to-ground) motor terminal overvoltage and CM stator neutral overvoltage (motor neutral to ground). Both the high switching speed (high *dv/dt*) effect and the high switching frequency effect on the motor overvoltage are investigated in this paper, where the high switching frequency effect has not been fully addressed in existing literature. Significant overvoltage is observed when the switching frequency or its multiples coincide with the cable or motor anti-resonant frequency. The anti-resonant behavior in the cable and motor impedance has been used to identify the overvoltage oscillation frequency and to explain the overvoltage observations for the three types of motor overvoltages. The analysis has been tested using a 7.5kW motor setup with and without a four-core cable, driven by a SiC or a GaN three-phase inverter with a switching frequency up to 250kHz and switching speed up to 40kV/μs. In addition, the motor bearing current, which is a main cause of bearing degradation, has also been tested and the increase of bearing current is observed due to the high frequency effect.

INDEX TERMS Anti-resonance, bearing currents, common-mode, differential mode, motor drive, motor overvoltage, neutral point voltage, gallium-nitride (GaN), silicon-carbide (SiC), switching frequency, switching speed, wide-bandgap.

I. INTRODUCTION

With the superior characteristics and commercial availability, wide-bandgap (WBG) devices are gradually finding their applications. Compared to silicon (Si) counterparts, silicon-carbide (SiC) and gallium-nitride (GaN) devices have faster switching speeds (shorter switching time), higher switching frequencies, higher voltage blocking capability and higher temperature performance [1], [2]. The switching frequency of WBG inverters can reach 100s of kHz and the rise time of the switching voltage can be as short as 10s of nanoseconds for SiC devices and less than 10ns for GaN devices [3]. In contrast, the switching frequency of Si IGBT inverters is normally below 20 kHz and the switching time is in the order of several hundred nanoseconds or even longer. Higher switching frequency can reduce the filtering components and the faster switching speed can reduce the switching loss, hence the cooling requirement [4], [5]. The adoption of WBG devices in motor drive systems can improve power density and efficiency and enable high-fundamental-frequency drives for electric machines with high-speed and high number of poles. This is favored in

The associate editor coordinating the review of this manuscript and approving it for publication was Zhixiang Zou.

high-efficiency and high-power-density applications such as more electric aircrafts and electric vehicles.

However, under high-switching speed (high *dv/dt*) and high-switching frequencies, the motor experiences overvoltage at both its terminals [6] and its neutral point [7], [8]. These overvoltages stress the motor winding insulation and bearings, which may lead to degradation and pre-mature failure. Furthermore, under high *dv/dt*, the voltage (including the overvoltage) distributes unevenly across the motor windings and normally the first several turns of the winding encounter most of the overvoltage, which further stress the insulation of the first several turns [9]. The cause of the overvoltages is mainly due to the impedance mismatch. For example, at the motor terminals, the motor surge impedance is much higher than the cable (between the inverter and motor) surge impedance, and hence the overvoltage is generated due to the reflected wave phenomenon. This motor terminal overvoltage appears in both the phase-to-phase voltage (differential mode (DM)) and phase-to-ground voltage (common-mode (CM)). Similarly, for the motor stator neutral, as the neutral point is normally floating, the CM impedance of the motor is facing an open circuit (infinite impedance to ground) at the motor neutral. Therefore, there is also an impedance mismatch at the motor neutral, so there is an overvoltage between the motor neutral and ground, again due to the voltage reflection phenomenon. However, there is no DM overvoltage at the motor neutral because the three phases are shorted together at the neutral point. To the authors' knowledge, the above points are articulated in this paper for the first time in literature based on the authors' understanding on this topic and will be explained in more detail in this paper. In summary, there are three types of overvoltages, the DM (phase to phase) and CM (phase to ground) overvoltages at the motor terminals and the CM overvoltage (neutral to ground) at the motor neutral.

To protect motor stator winding insulation, the slew rate (*dv/dt*) of the motor input voltage is suggested to be limited to 500 V/μs by the standards, e.g., MG1 of National Electrical Manufacturers Association (NEMA) for general motors [10]. However, the motor terminal is subject to much higher voltage slew rate (e.g., $>$20kV/μs) and more serious overvoltage when the WBG devices are used. For example, for a 600V inverter dc-link voltage, a typical switching speed of 30ns with SiC MOSFETs leads to a *dv/dt* of 20V/ns (20kV/μs) in the phase-to-phase voltage. Furthermore, under higher switching speeds, the overvoltage at motor terminals can reach twice of the inverter output voltage when there is a cable connected between the inverter and the motor, due to the voltage reflection phenomenon [11], [12]. This overvoltage phenomenon has been observed for conventional Si IGBT based motor drives with long cables (tens or hundreds of meters). However, with the very fast switching of WBG devices, the cable length that can lead to overvoltage has been reduced to several meters [13]. Further, under high switching frequencies, a greater than twice of the inverter voltage can occur at the motor terminal at high modulation indices. This is known as the double pulsing effect, where a second voltage pulse arrives at the motor terminals before the first reflected pulse is fully decayed under closely spaced PWM pulses [11], [14], [15], causing higher than double the inverter output voltage at the motor terminal.

The negative impact of fast-switching WBG devices and inverters has drawn significant attention with the increasing adoption of WBG devices in various motor drive applications, such as electric vehicles [16]. The overvoltage due to the reflected wave phenomenon with GaN HEMTs, SiC MOSFETs and Si MOSFETs are studied and compared in [4]. It has been found that the motor overvoltage is more likely to happen under shorter rise time of the inverter output voltage. The motor winding overvoltage can incept partial discharges that progressively yield to the degradation of polyamide-imide and polyester coating of motor coils [17]. The high voltage slew rate (high *dv/dt*) due to fast-switching and the high switching frequency increases the capacitive-type bearing current and affect the electric discharge machining (EDM) bearing current [18]. These bearing currents are the root cause of bearing degradation and failure.

Regarding the mitigation of the high *dv/dt* and its negative impact on electric machines, several approaches have been introduced in literature to mitigate the motor overvoltage in cable-fed drives. Among them, the off-the-shelf mitigation approach is employing passive filters either at the inverter side, motor side, or both sides to suppress the overvoltage transients at the motor terminals. Different passive filter designs have been investigated in various studies under two categories: *dv/dt* filters and impedance matching filters [19]. The *dv/dt* filters reduce the overvoltage transients by limiting the voltage derivative applied to the system. Whereas, the impedance matching filters alleviate the impedance difference between the cable and motor. Although passive filters can eliminate the motor overvoltage transients, they induce additional volume/weight and power loss in the drive system, countering the advantages of WBG devices. They also add cost to the system. Moreover, the passive elements of some filter networks are specifically designed for a certain cable length, where the variation of the cable length requires re-designing the filter parameters.

To avoid the shortcomings of passive filters, methods have been proposed to attenuate the *dv/dt* or harmonics from the source, i.e., by shaping the output voltage waveforms of the inverter. A soft-switching converter has been introduced to shape the SiC inverter output voltage to have a longer rising/falling time that can mitigate the motor terminal overvoltage [13]. It has been found that when the rising/falling time of the inverter output voltage is four times of the voltage wave propagation time along the cable, the motor terminal overvoltage can be fully attenuated. Multi-level converters can also be used to attenuate the motor

terminal overvoltage since there are more steps in the output voltage, hence less *dv/dt* [16]. The amplitude of the voltage overshoot at the motor terminal is proportional to the voltage change (ΔV) of the inverter output voltage, where multi-level converters have a lower voltage change (ΔV), hence can attenuate the motor terminal overvoltage. A quasi-three-level modulation method was presented in [12], which can attenuate the motor overvoltage by introducing an intermittent voltage level to the standard two-level converter. The quasi-three-level modulation can significantly counteract the reflected wave phenomenon, hence reducing the overvoltage at motor terminal. In [20], mitigation of CM noise from SiC converters using filters and open-end winding configurations has been reported.

Although existing literature has analyzed the overvoltage phenomenon due to the high switching speed (high *dv/dt*) of WBG devices, the effect of high-switching frequency of WBG devices on the overvoltage has not been well discussed in literature. With WBG device-based motor drives, the switching frequency can reach 40kHz or even 100s of kHz if needed. If this high-switching frequency or its associated harmonics at multiples of the switching frequency or their sidebands coincide with the anti-resonant frequency of the cable or/and the electric machine, then there is much higher overvoltage than those due to the high *dv/dt* (switching speed) effect. These switching-frequency-driven effects have been analyzed in detail in this paper. Also, the impedance-based method with anti-resonant frequency is used to analyze the effects due to high *dv/dt*, high-switching frequency and the overvoltage oscillation frequency can be directly analyzed and obtained with the anti-resonant frequency. Essentially, the *dv/dt* driven overvoltage/oscillations exhibit travelling wave phenomenon while the switching-frequency driven overvoltage/oscillations exhibit standing wave phenomenon. Both the CM and DM overvoltage at the motor terminal and the CM overvoltage at the motor neutral are systematically presented for the first time in this paper.

This paper aims to provide a timely investigation and useful reference for the impact of high-switching speed and high-switching frequency WBG motor drives on electric machines. The remainder of this paper is structured as follows. Section II analyzes the factors influencing the motor overvoltage using the wave reflection theory in the time domain and the impedance-base method in the frequency domain. Section III lays out the three types of motor overvoltages, including the DM and CM motor terminal overvoltage and the CM motor stator neutral overvoltage. The impact of switching speed and switching frequency on these three types of overvoltages is investigated in detail. Section IV shows the impact of high *dv/dt* and high-switching frequency on the motor bearing current. Experimental results with a SiC MOSFET inverter and a GaN HEMT inverter based motor drive and an induction motor are embedded in the above sections to validate the analysis. Section V concludes the paper.

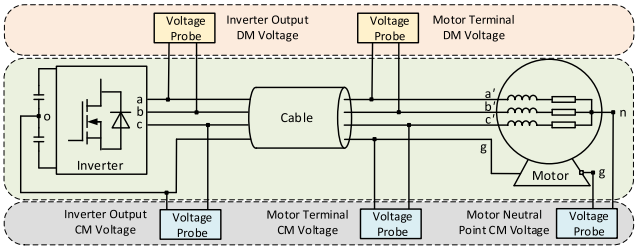

FIGURE 1. Schematic of a variable speed motor driver system.

II. MOTOR OVERVOLTAGE ANALYSIS IN THE TIME DOMAIN AND FREQUENCY DOMAIN

In this section, the motor terminal overvoltage and neutral point overvoltage using the time-domain analysis (wave reflection phenomenon) and frequency-domain analysis (anti-resonant frequency) are introduced. First, the structure of a variable speed motor drive system is shown in Fig.1. Here, the inverter is assumed to be based on WBG (SiC, GaN) devices but the analysis can also be used for Si devices such as Si IGBTs. The inverter is connected to the motor through a cable (inverter-cable-motor system). It should be noted that the motor terminal overvoltage is a result of the existence of the cable between the inverter and motor. But the motor neutral overvoltage is not caused by the cable and can occur without any cable connected. In the structure shown in Fig.1, the inverter dc-link capacitor midpoint (o) is connected to the motor case via a ground wire (g). In this way, the inverter CM voltage directly drops across the motor stator neutral (n) and the ground (motor case), i.e., o, g, where o and g have the same potential. In some applications, the inverter dc-link neutral point (o) is not directly connected to the earth. Therefore, the CM voltage drops between the motor stator neutral and inverter dc-link neutral linked by the parasitic capacitance between the inverter neutral and the earth/ground. Fig.1 also shows how various inverter/motor voltages are measured.

Fig.2 shows the experimental setup for evaluating the impact of high switching speed and high switching frequency of WBG motor drives on electric machines. Here, a 7.5kW inductor motor-generator set was used as the test machines. A SiC MOSFET based three-phase DC/AC inverter and a GaN HEMT based one with tunable switching speed and switching frequency are used as the motor drive inverters. A cable (3.9m and 70m) is also connected between the inverter and motor as shown in Fig.2.

A. ANALYSIS USING THE WAVE REFLECTION PHENOMENON (TIME DOMAIN)

Fundamentally, the overvoltage is due to the wave reflection phenomenon, where there is a mismatch between the two surge impedances connected, i.e., one impedance is much larger than the other. This explains why there is motor terminal overvoltage, i.e., the motor surge impedance is much higher than the cable surge impedance. This also explains why there is motor stator winding neutral point

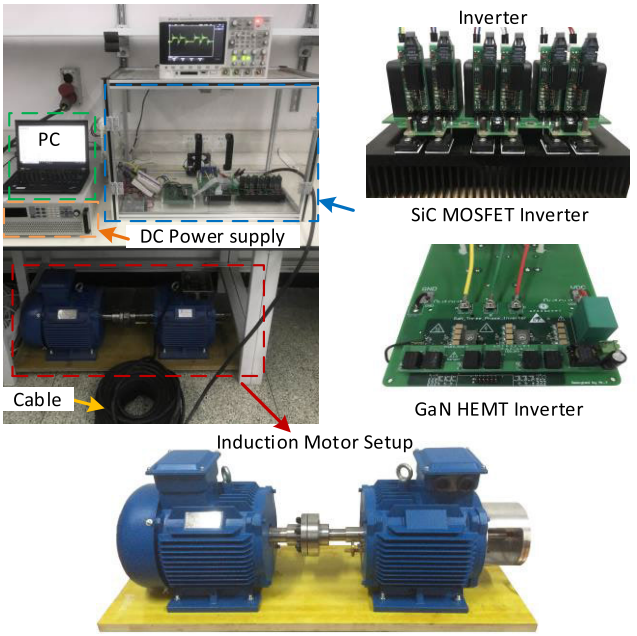

FIGURE 2. Photo of the experimental setup and its components.

overvoltage, i.e., the motor neutral is facing an infinite large CM impedance (open circuit). Fig. 3 illustrates the impedance mismatch that causes the motor terminal DM and CM overvoltage and the motor neutral CM overvoltage. Note that there is no DM overvoltage at the motor neutral because the three phases are short-circuited together at the neutral. In other words, the DM voltage at stator neutral is zero.

Considering the motor terminal DM overvoltage as an example, using the wave reflection theory, there are three main factors influencing the overvoltage magnitude at the motor terminal, which are the cable length, rise time of the inverter output voltage pulses (PWM pulses), and surge impedance mismatch between the cable and motor. The forward travelling voltage wave from the inverter through the cable generates a reflection wave after arriving at the motor terminal and the magnitude is scaled by the reflection coefficient [21], with a maximum value of 2, which means the motor terminal voltage (DM) doubles the inverter output voltage (DM). The cable critical length is defined as the length where the maximum overvoltage (double in a worst) occurs and any cable length longer than the critical length generates the maximum overvoltage. Hence, with cables, the motor terminal overvoltage peak (V_{peak}) can be given by (1).

$$V_{\text{peak}} = V_{\text{dc}} N_{\text{m}} + V_{\text{dc}} \tag{1}$$

where, V_{dc} is the magnitude of the forward wave and is equal to the inverter dc-link voltage, N_{m} is the reflection coefficient at the motor terminal which can be expressed as a function of the cable surge impedance (Z_{c}) and the motor surge impedance (Z_{m}) as shown in (2) and (3. The maximum value of N_{m} is 1, meaning the motor surge impedance is much

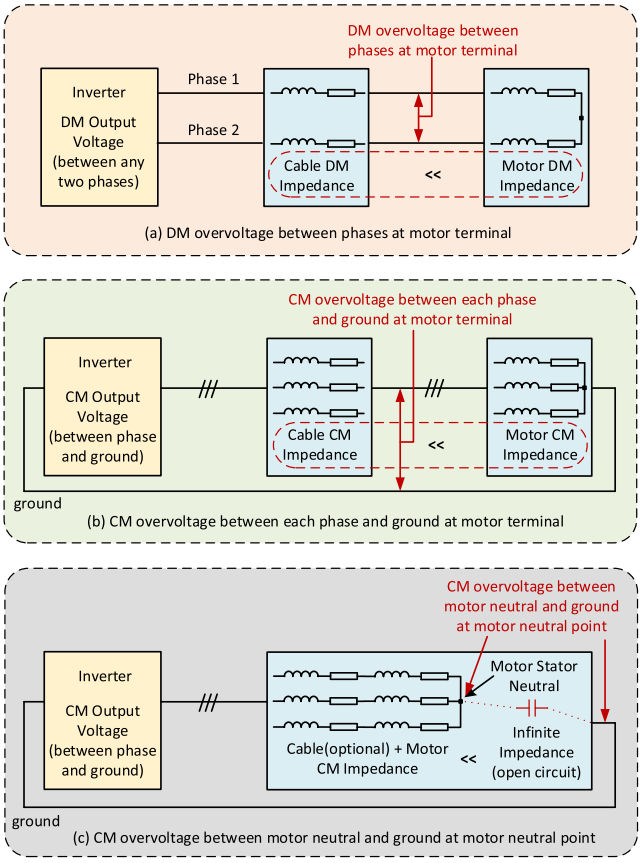

FIGURE 3. Illustration of three types of overvoltages due to impedance mismatch: (a) DM overvoltage between phases at motor terminal. (b) CM overvoltage between each phase and ground at motor terminal. (c) CM overvoltage between motor neutral and ground at motor neutral point.

larger than the cable surge impedance.

$$N_{\text{m}} = (Z_{\text{m}} - Z_{\text{c}}) / (Z_{\text{m}} + Z_{\text{c}}) \tag{2}$$

$$Z_{\text{c}} = \sqrt{\frac{L_0}{C_0}} \tag{3}$$

In (3), L_0 and C_0 are inductance and capacitance per unit cable length, respectively. The cable surge impedance Z_{c} is closely related to the structure, material and parasitic parameters. The value of the motor surge impedance Z_{m} can be approximated according to empirical formula (around 400 Ω for a 7.5kW motor) [22], which is normally higher than the cable surge impedance.

For cables that are shorter than the critical length, the motor overvoltage is affected by the rise time (t_{r}) of the inverter output voltage. The propagation of the traveling waves along the cable from the inverter output to the motor terminal takes time, which is defined as t_{p}. Hence, the motor terminal overvoltage peak (V_{peak}) with short cables can be given by (4) [21]

$$V_{\text{peak}} = \frac{3lV_{\text{dc}}N_{\text{m}}}{vt_{\text{r}}} + V_{\text{dc}} \tag{4}$$

where, l is the cable length, v is the pulse velocity in the cable, t_{r} is the rise time of the inverter output voltage.

The voltage pulse propagation time (t_p) can be expressed as the function of l and v as shown in (5).

$$t_p = \frac{l}{v} \tag{5}$$

The pulse propagation velocity (v) relates to the inductance (L_0) and capacitance (C_0) of per unit cable length [23]. Besides, the pulse propagation velocity can also be defined as a function of the permeability (μ) and permittivity (ε) of the dielectric material between conductors [24]. Hence, v can be expressed as (6).

$$v = \frac{1}{\sqrt{L_0 C_0}} = \frac{l}{\sqrt{\mu\varepsilon}} \tag{6}$$

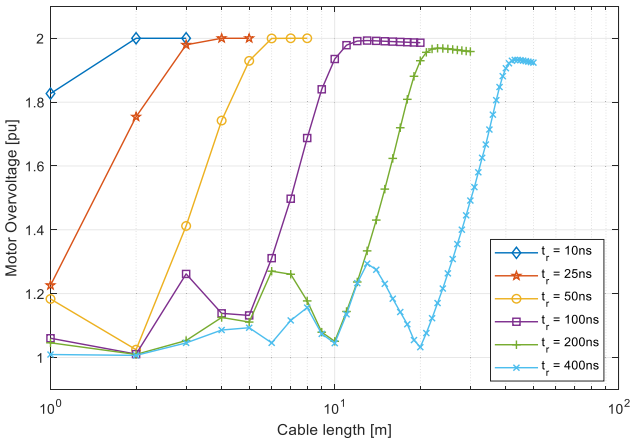

FIGURE 4. The relationship between motor terminal overvoltage and cable length under various switching speeds [26], [27].

The theoretical prediction in (1) and (4) can provide an approximated overvoltage value. Further, a simulation has been carried out with distributed cable parametric models to find the relationship between the terminal overvoltage value and the cable length under various switching speeds [25]. The results are shown in Fig.4. As seen, under a standard switching speed of 25ns of SiC MOSFETs, the critical cable length that generates maximum overvoltage (double in this case) is only 4 meters. For GaN HEMTs with a 10ns switching speed, the critical length is just a couple of meters. This length is much shorter than those used in Si IGBT based motor drives, where the cable critical length is around tens of meters with Si IGBT switching speeds between several hundreds of ns and few μs. Therefore, the overvoltage due to the fast-switching of WBG devices need serious attention even with very short cables of several meters.

Also, the wave reflection phenomenon can be analyzed using the so-called bounce diagram as shown in Fig.5 [6], which shows how a travelling wave bouncing between the inverter and motor terminal with the reflection coefficients being N_s and N_m, respectively. From Fig.5, it can be seen that the period of the overvoltage is $4t_p$ and hence the oscillation frequency of the overvoltage is $1/(4 \times t_p)$.

Fig. 6 shows the measured voltages using a SiC inverter and a 70m long cable. One end of the cable is connected

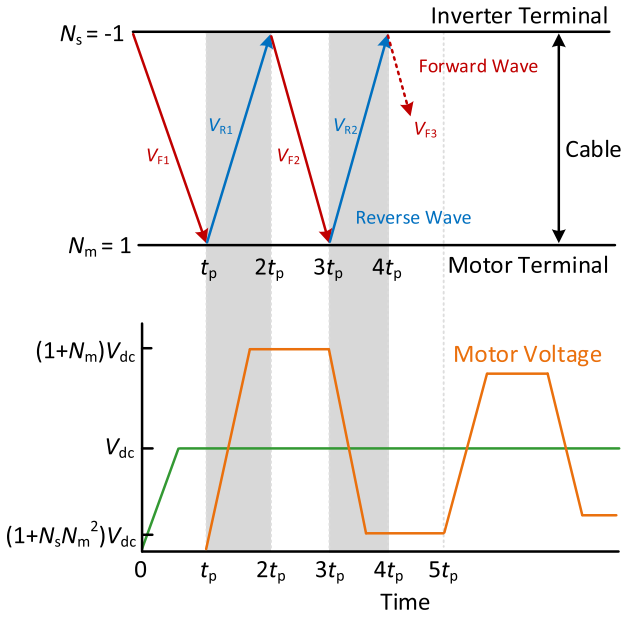

FIGURE 5. Illustration of motor terminal overvoltage using bounce-diagram.

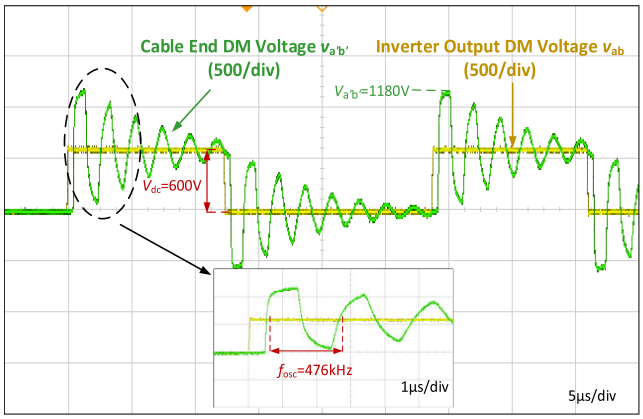

FIGURE 6. Inverter output voltage v_{ab} and cable end voltage $v_{a'b'}$ with a 70m cable: dc-link voltage=600V, switching frequency=10kHz.

to the inverter and the other end is open circuit to emulate the high impedance of the electric machine. As seen, there is clear overvoltage at the open-circuit (motor) end and the peak value has reached twice of the inverter output voltage. Here, the inverter dc-link voltage (V_{dc}) is 600V and hence the magnitude of the inverter output DM voltage (v_{ab}) is also 600V. As seen, the cable end DM voltage $v_{a'b'}$ has reached 1180V. Based on the measured cable parameters using an impedance analyzer, $L_0 = 462$nH/m, $C_0 = 122$pF/m and from (6), the wave travelling speed in the cable can be calculated as 1.332×10^8m/s. Hence, the propagation time (t_p) through the cable is 525.53ns. Based on Fig.5, the calculated oscillation frequency of the overvoltage is 475.71kHz ($1/(4 \times t_p)$), which agrees with the measured oscillation frequency of 476kHz as shown in Fig.6.

In addition, Fig.7 shows the cable end overvoltage with a 3.9m short cable and a switching speed of 60ns of the SiC inverter. As seen, the overvoltage has reached 1100V,

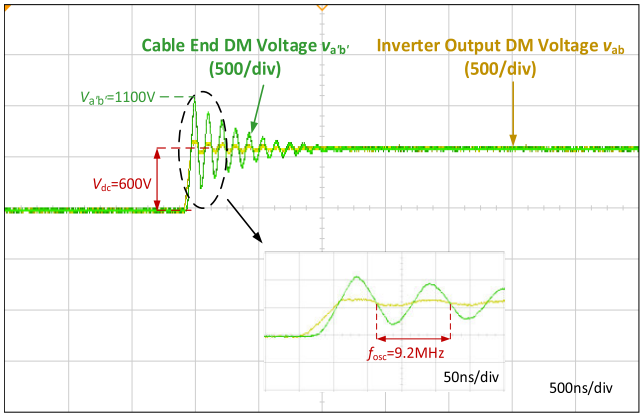

FIGURE 7. Inverter output voltage v_{ab} and cable end voltage $v_{a'b'}$ with a 3.9m cable: dc-link voltage=600V, switching frequency=10kHz.

much higher than the 600V inverter output voltage and the result is in agreement with the results given in Fig.4. Also, the oscillation frequency (9.2MHz) is much higher than the long cable case.

B. ANALYSIS USING THE IMPEDANCE-BASED APPROACH (FREQUENCY DOMAIN)

Though the time domain based wave reflection analysis presented above can be useful in analyzing simple systems such as cables, it may not be straightforward to be used in analyzing more complicated systems such as electric machines due to their more complicated parasitic elements, coupling and high-frequency effects. Hence, impedance-based analysis with direct impedance measurement can be more straightforward and useful in identifying the anti-resonant frequency of the system, which can be used to predict the oscillation frequency of the overvoltage. Furthermore, this impedance-based method clearly shows which switching frequency driven harmonics excites large resonant and overvoltage due to their collision with the anti-resonant frequency.

Fig.8 shows how the CM and DM impedance of the cable, motor and cable+motor systems can be measured using an impedance analyzer. It should be noted that the measurement diagram shown in Fig.8 is slightly different to the commonly used open-circuit and short-circuit test for extracting parameters. The CM and DM impedance measurement shown in Fig.8 represents the real/physical connection of the motor drive system.

Fig.9 shows the DM impedance measurement results for the cable, motor and cable+motor, which are measured according to the diagram shown in Fig.8. Fig. 9(a) shows the cable DM impedance, which has an anti-resonant frequency of 476kHz. This frequency precisely matches the oscillation frequency of the overvoltage shown in Fig.6. Hence, this impedance-based method can be used to predict the oscillation frequency. Also, this anti-resonant frequency tells which switching frequency related harmonics (excitation source) should be avoided, thus not to coincide with the

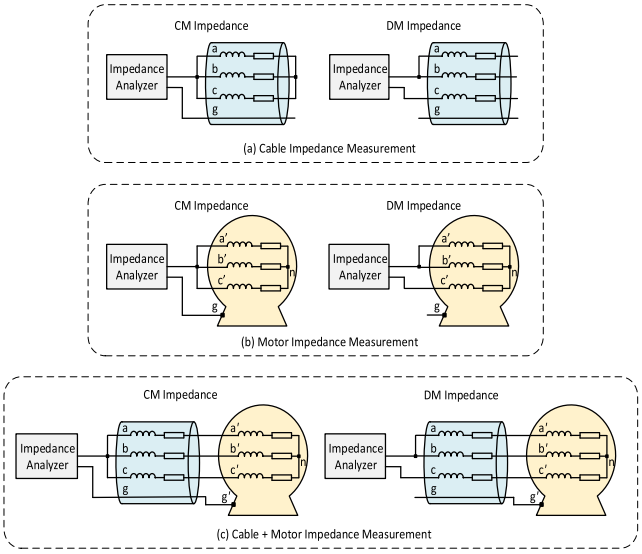

FIGURE 8. Impedance measurement of the cable, motor and cable+motor: (a) Cable impedance measurement, (b) Motor impedance measurement, (c) Cable+motor impedance measurement.

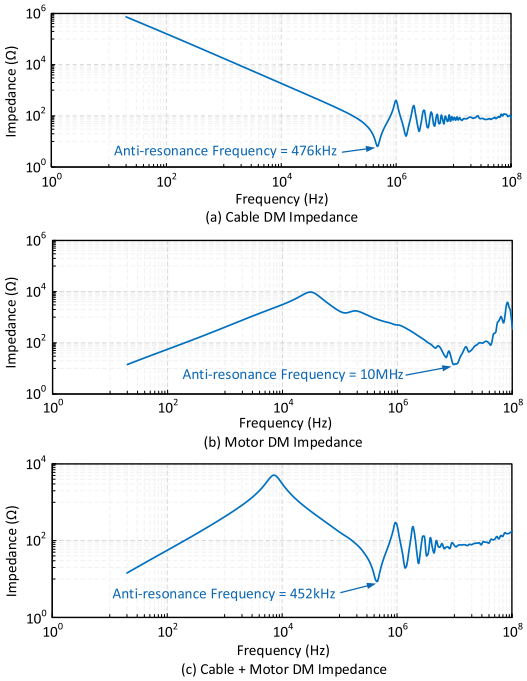

FIGURE 9. DM impedance measurement results: (a) Cable DM impedance, (b) Motor DM impedance, (c) Cable+motor DM impedance.

anti-resonant frequency. Otherwise, there will be very high overvoltage magnitude due to the very low impedance at this frequency. How Fig.9 (b)(c) can be used to analyze and predict the DM overvoltage at the motor terminal due to the *dv/dt* and switching frequency effect will be given in the next section (section III).

Fig.10 shows the CM impedance measurement results for the cable, motor and cable+motor, again according to the measurement diagram shown in Fig.8. How these can be used to analyze and predict the CM overvoltage at the motor

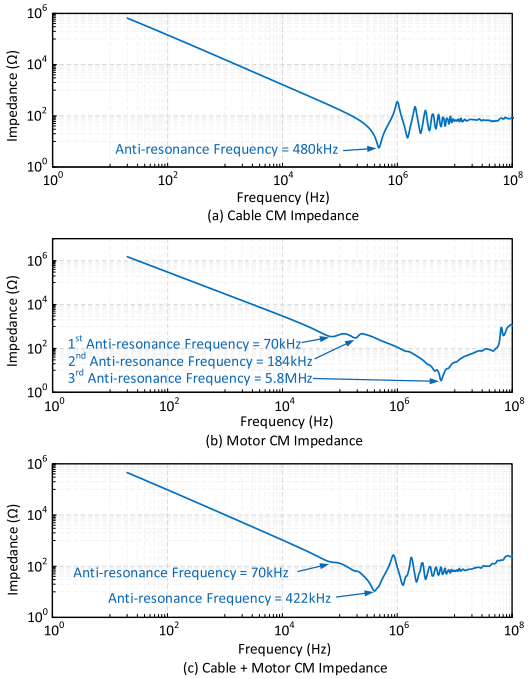

FIGURE 10. CM impedance measurement results: (a) Cable CM impedance, (b) Motor CM impedance, (c) Cable+motor CM impedance.

terminal and stator neutral will also be given in the next section.

III. THREE TYPES OF MOTOR OVERVOLTAGE

As mentioned, there are three types of motor overvoltages, i.e., DM and CM overvoltage at the motor terminal and CM overvoltage at the motor neutral, which has been discussed and experimentally shown in this section considering both the *dv/dt* effect and the switching frequency effect. It also shows how the experimental observations agree with the impedance-based analysis.

A. MOTOR TERMINAL OVERVOLTAGE (DM & CM)

There is motor terminal overvoltage between the phases of the motor (DM) and between each phase and ground (CM) because the impedance of the machine is much higher than the cable. Here, a 70m cable is connected between the inverter and the motor and the GaN converter is used here with a dc-link voltage of 50V. The modulation index is 0.9.

Fig.11 shows the DM overvoltage at the motor terminal. The overvoltage is almost twice of the inverter voltage and the oscillation frequency agrees with the measured impedance anti-resonant frequency of 452kHz as shown in Fig.9(c).

Fig.12 shows the motor terminal CM voltage (phase to ground voltage). As seen, the inverter output voltage jumps between negative half of the dc-link voltage (−25V) to the positive half of the dc-link voltage (25V). The CM phase to ground voltage overshoot is about 40V higher than the inverter output voltage of 25V. Also, the oscillation frequency agrees with the CM impedance anti-resonant frequency of 422kHz as Fig.10 (c).

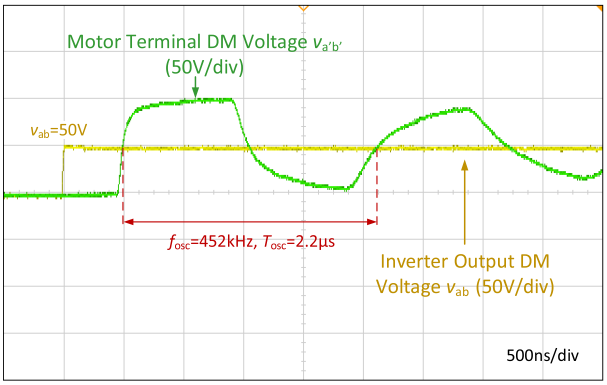

FIGURE 11. Motor terminal DM overvoltage: dc-link voltage=50V, switching frequency=10kHz.

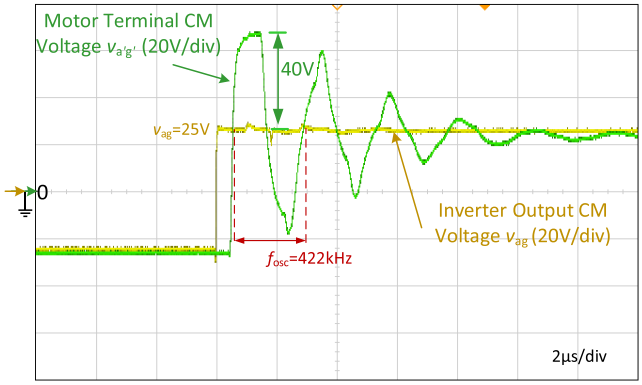

FIGURE 12. Motor terminal CM overvoltage: dc-link voltage=50V, switching frequency=10kHz.

The following shows how the switching frequency affects the DM and CM motor terminal overvoltage. Fig.13 shows the variation of the motor terminal overvoltage with respect to the switching frequency and Fig.14 shows the transient details. As seen in Fig.13, the switching frequency increases from 10kHz to 250kHz using the GaN inverter and the overvoltages show different behaviors and have different magnitude at various switching frequencies. At 10kHz, the overvoltage is due to the standard wave reflection phenomenon and the motor terminal overvoltage magnitude is around twice (i.e., 105V) of the inverter output voltage. At 50kHz, the magnitude has further increased to be higher than double the inverter output voltage, i.e., 139V. This is mainly due to the double pulsing effect, where at high switching frequencies and high modulation indices, the pulses are closely spaced. As a result, the overvoltage due to the first pulse has not fully decayed and the overvoltage due to the following pulses adds on top of it as shown in Fig.14(b), causing further overvoltage. With 150kHz switching frequency, as shown in Fig.13(c) and Fig.14(c), the overvoltage magnitude has further increased to 213V, which is more than four times of the inverter output voltage and puts significant stress on the winding insulation. Here, the 50V inverter dc-link voltage is used to make sure the overvoltage does not damage the machine under test. This very high overvoltage is mainly due to the fact that the triple

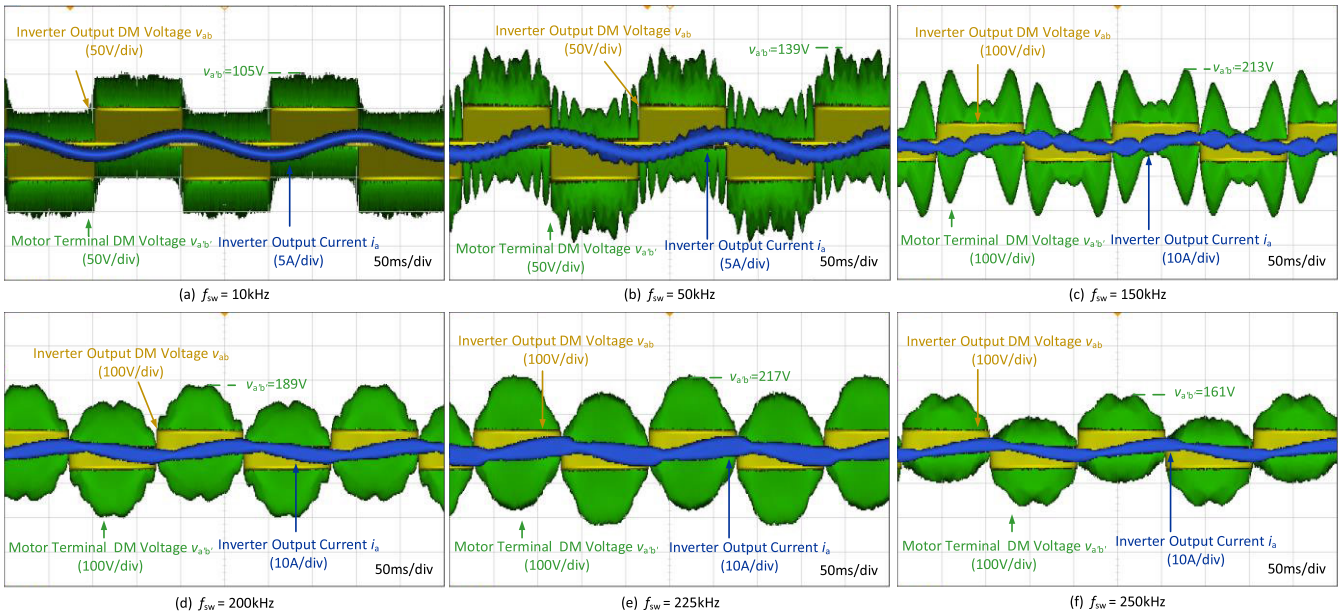

FIGURE 13. The variation of motor terminal DM overvoltage with switching frequency: modulation index=0.9, dc-link voltage=50V.

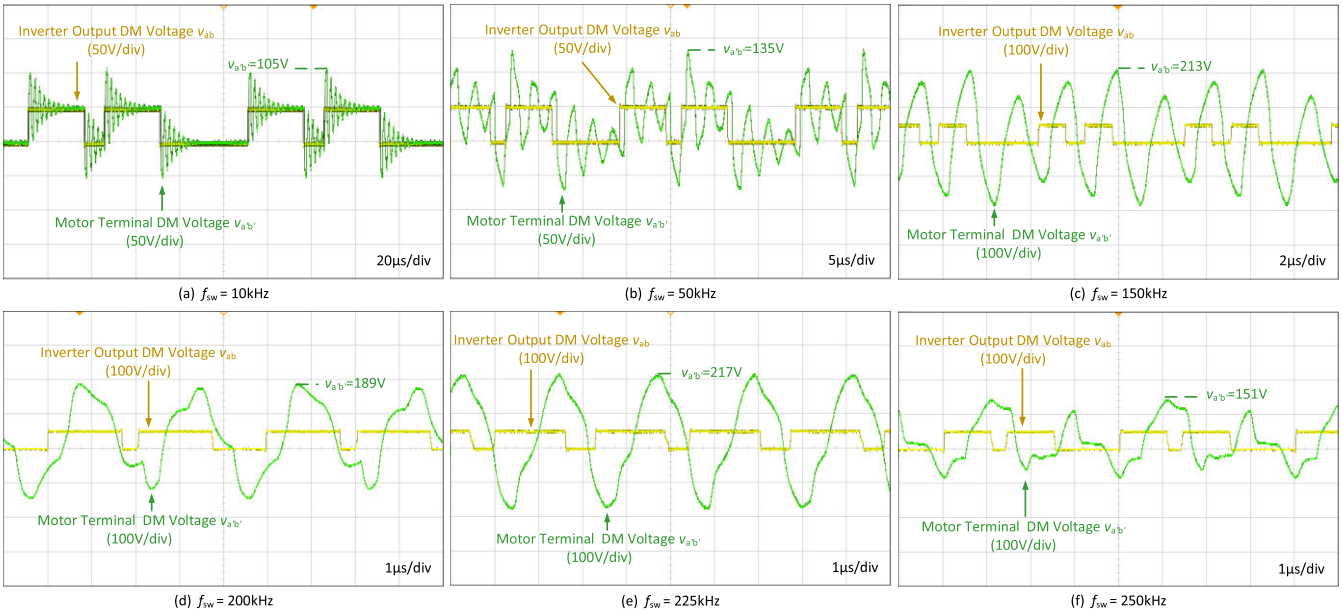

FIGURE 14. Close-up view of the motor terminal DM overvoltage waveforms in Fig.13.

harmonics of the 150kHz, i.e., 450kHz and its side-band harmonics matches the anti-resonant frequency of the DM impedance as shown in Fig.9(c), i.e., 452kHz, hence causing a very large overvoltage spike. Therefore, the impedance-based analysis is very useful to predict which switching frequencies may excite very high motor overvoltage and hence should be avoided. Similarly, for the switching frequency of 225kHz, the overvoltage is very high, i.e., 217V due to the same reason. At 200kHz and 250kHz, the overvoltage is slightly lower because the multiples of these switching frequencies do not fall on the anti-resonant frequency. Nevertheless, the double pulsing effect still cause a higher overvoltage. Furthermore, it can be seen from Fig.13 that the current has been clearly distorted when there is overvoltage, which may cause harmonic losses, torque ripple, etc.

Although, in practical applications, the switching frequency is unlikely to be higher than 100kHz for motor drives, the high switching frequency effect shown here can effectively reflect what will happen when the cable length is much longer, e.g., hundreds of meters, where 10s of kHz switching frequency in that case has a similar effect to what have been shown in Fig.13 and Fig.14.

Fig.15 and Fig.16 show the variation of motor terminal CM overvoltage (phase to ground) with the switching frequency.

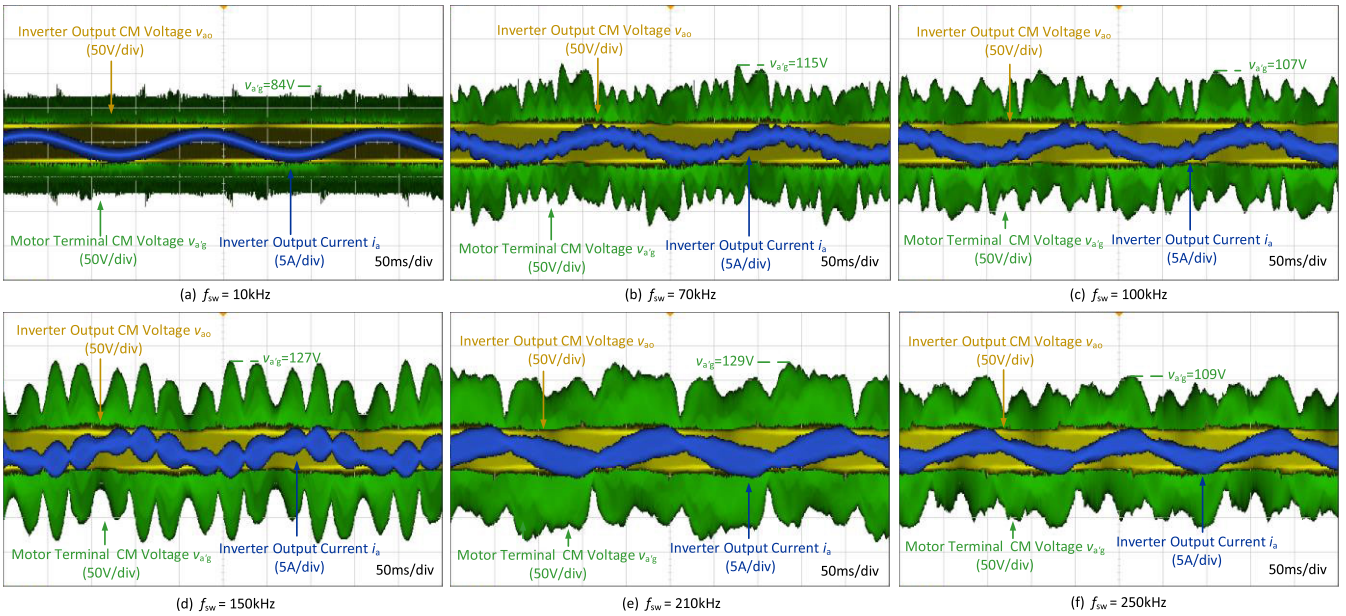

FIGURE 15. The variation of motor terminal CM overvoltage with switching frequency: dc-link voltage=50V, modulation index=0.9.

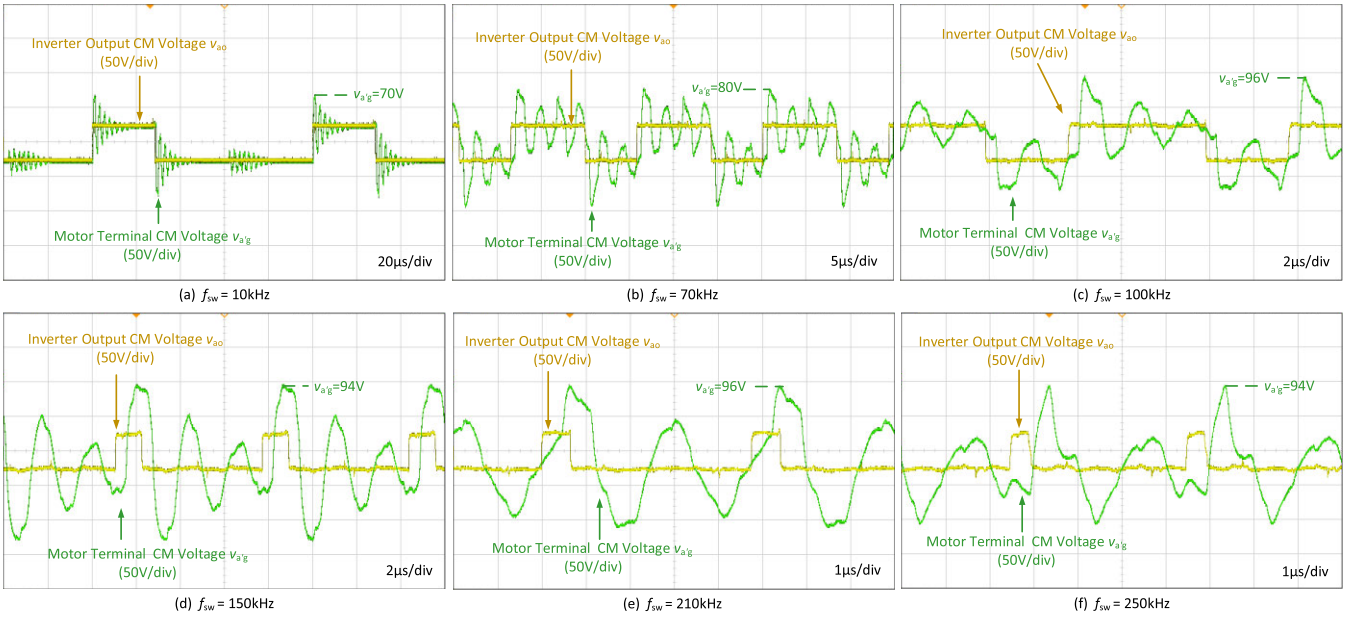

FIGURE 16. Close-up view of the motor terminal CM waveforms in Fig.15.

It shows similar phenomenon as what has been observed for the DM motor terminal overvoltage and it can be explained using the same analysis for the DM overvoltage discussed above. As mentioned, the first several turns of the stator winding that are close to the motor terminal faces the highest DM and CM overvoltage stress.

B. MOTOR NEUTRAL OVERVOLTAGE (CM)

The third type of overvoltage occurs at the motor stator winding neutral and is between the neutral and ground (CM overvoltage) due to the fact that the stator neutral is facing an open-circuit (infinite impedance) to ground. And the last several turns close to the neutral experiences high CM overvoltage. This overvoltage is driven by the CM voltage generated by the inverter, as defined in (7).

$$v_{\mathrm{CM}} = (v_{\mathrm{ao}} + v_{\mathrm{bo}} + v_{\mathrm{co}})/3 \tag{7}$$

where, v_{cm} is the CM voltage generated by the inverter, v_{ao}, v_{bo} and v_{co} are the phase output voltages with respect to the dc-link neutral point (o), with values of $+V_{\mathrm{dc}}/2$ or $-V_{\mathrm{dc}}/2$, depending on the switching state.

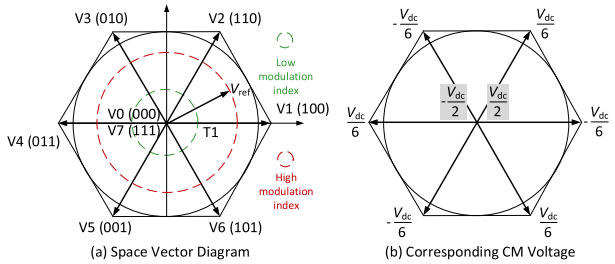

FIGURE 17. Space vector diagram and its corresponding CM voltages.

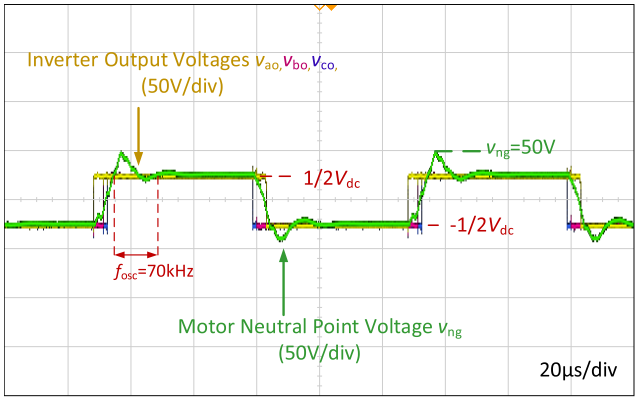

(a) Neutral point voltage and inverter output voltages (v_{ao}, v_{bo}, v_{co}).

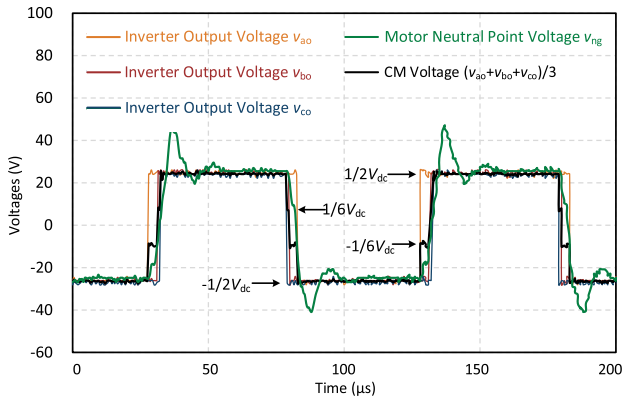

(b) Waveforms in (a) replotted and with the CM voltage added

FIGURE 18. Motor stator neutral overvoltage with a modulation index of 0.1 and dc-link voltage=50V, switching frequency of 10kHz.

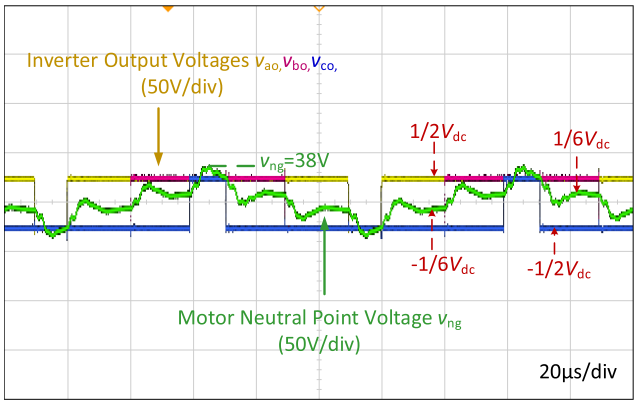

(a) Neutral point voltage and inverter output voltages (v_{ao}, v_{bo}, v_{co}).

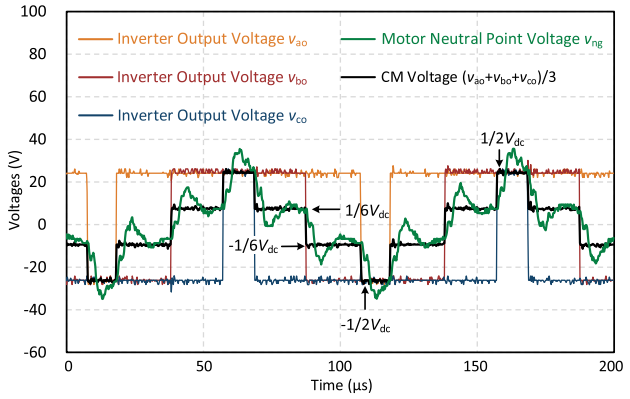

(b) Waveforms in (a) replotted and with the CM voltage added.

FIGURE 19. Motor stator neutral overvoltage with a modulation index of 0.9 and dc-link voltage=50V, switching frequency of 10kHz.

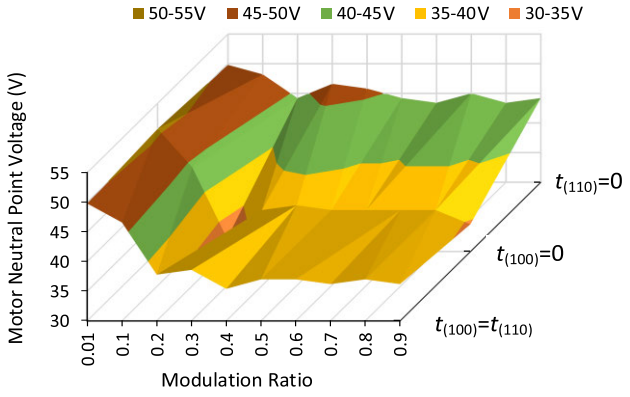

FIGURE 20. Variation of the motor neutral point voltage with modulation ratio and the location of the reference vector.

To better explain this CM neutral point overvoltage, Fig.17(a) shows the space vector modulation diagram of the two-level inverter, where there are in total 8 voltage vectors, including 6 active vectors and 2 zero vectors. In the switching states in Fig.17(a), 1 represents the top device of the phase leg is ON ($+V_{dc}/2$) and 0 represents the bottom device of the phase leg is ON ($-V_{dc}/2$). For example, (100) means Phase A top device is ON and Phase B and Phase C bottom devices are ON. Hence, according to (7), the corresponding CM voltages can be calculated as shown in Fig.17(b), with values of $+V_{dc}/2$, $-V_{dc}/2$, $+V_{dc}/6$, $-V_{dc}/6$.

It can be seen from Fig.17 that, when the modulation index is low, the two zero vectors (000) and (111) are used more and there are higher chances of the CM voltage being $+V_{dc}/2$ or $-V_{dc}/2$, hence larger CM voltage change and higher stator neutral point overvoltage. In contrast, when the modulation index is high, the CM voltage jump is smaller between $+V_{dc}/2$, $+V_{dc}/6$, $-V_{dc}/6$ and $-V_{dc}/2$, hence the voltage overshoot at the neutral point is smaller.

Fig.18 (a) shows the motor neutral point voltage (v_{ng}) and the three-phase inverter output voltages (v_{ao}, v_{bo}, v_{co}) at a low modulation index of 0.1. In this case, the inverter generated CM voltage has a higher jump to $1/2V_{dc}$ or

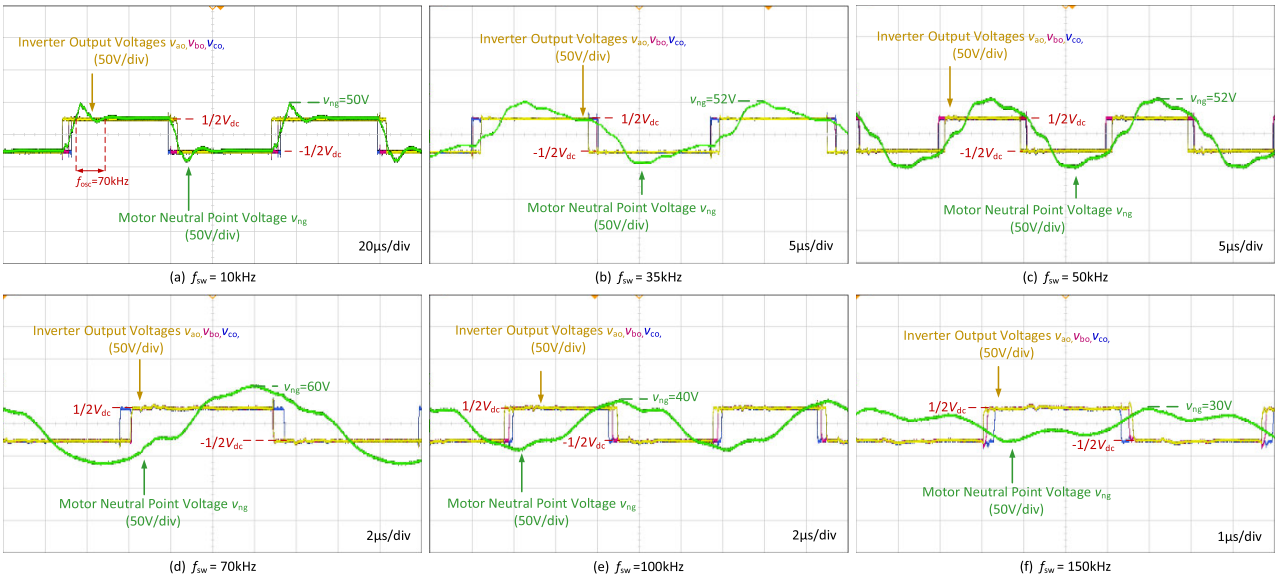

FIGURE 21. Motor neutral voltage with the variation of the switching frequency at modulation index=0.1.

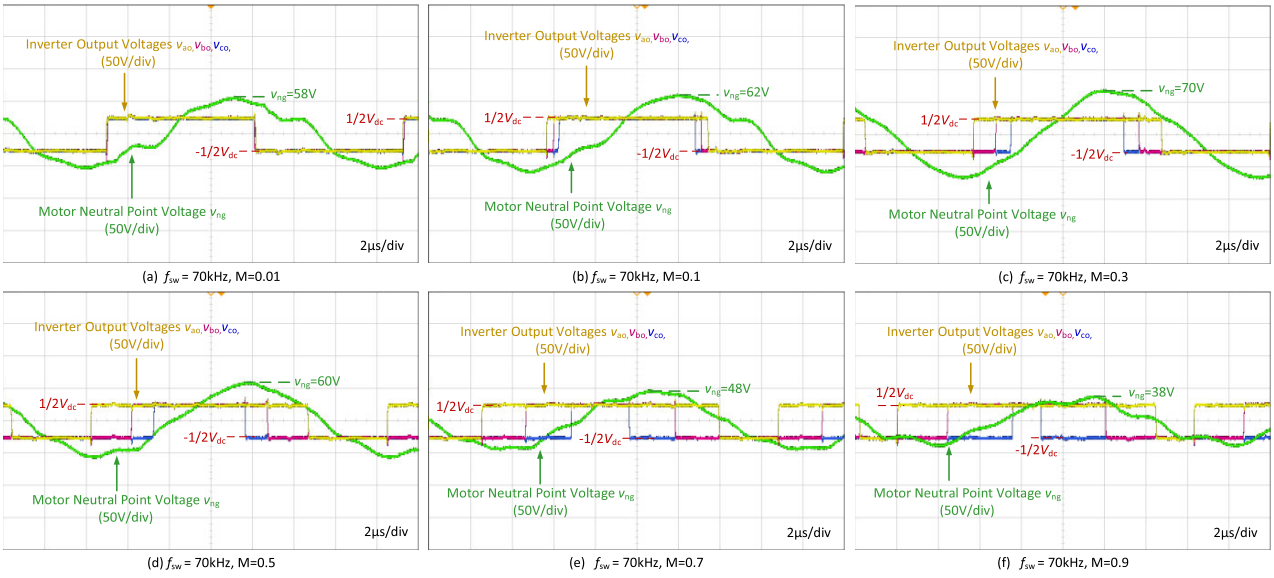

FIGURE 22. Variation of motor neutral overvoltage with the modulation indice: switching frequency=70kHz.

$-1/2V_{dc}$, hence resulting in a neutral point overvoltage as shown in Fig.18 (a), i.e., $v_{ng} = 50$V (which should be 25V without voltage overshoot). The oscillation frequency of the voltage overshoot is 70kHz, which agrees with the first anti-resonant frequency of the CM impedance shown in Fig.10(c), i.e., 70kHz. Fig.18 (b) further shows the CM voltage $(v_{ao} + v_{bo} + v_{co})/3$ with the black line in the figure. As seen, the time during the $1/6V_{dc}$ and $-1/6V_{dc}$ levels is very short, resulting in a higher voltage jump to $1/2V_{dc}$ and $-1/2V_{dc}$, hence higher voltage overshoot.

Fig.19 shows the motor neutral point voltage with a modulation index of 0.9. As seen, there are clear four steps $(+1/2V_{dc}, +1/6V_{dc}, -1/6V_{dc}, -1/2V_{dc})$ in the neutral point voltage and the overvoltage (38V) is lower than the case of 0.1 modulation index due to a smaller voltage jump.

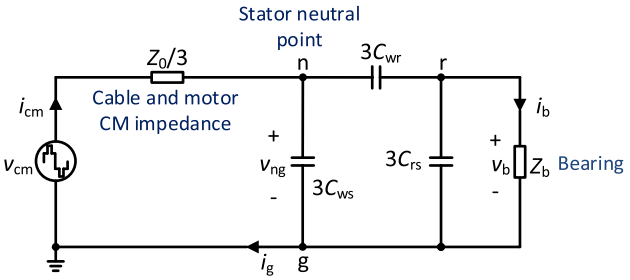

FIGURE 23. Diagram of the CM voltage and current path and the bearing voltage and current path.

It should be noted that apart from modulation index, the actual neutral overvoltage also depends on the location of the voltage reference vector (V_{ref}) as shown in Fig.17(a).

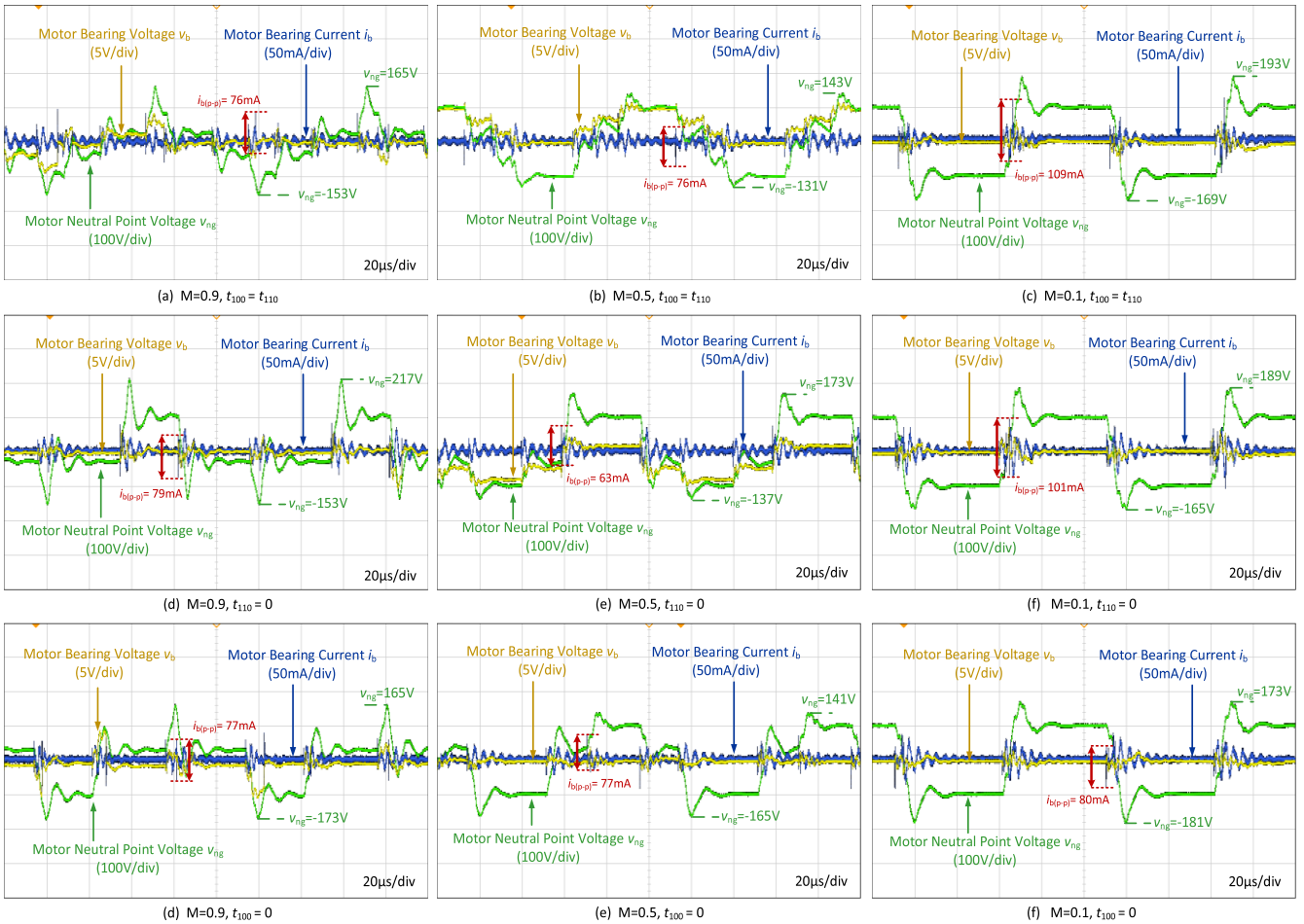

FIGURE 24. **Motor bearing current, bearing voltage and neutral voltage: dc-link voltage = 200V, switching frequency=10kHz and motor speed=150rpm.**

The location of V_{ref} determines which vectors are used more. For example, in Fig.17(a), if V_{ref} is aligned with V1, then only V1 (100), V0 (000) and V7 (111) are used to synthesize V_{ref}. If V_{ref} is located between V0 and V7, all the four vectors V1 (100), V2 (110), V0 (000) and V7 (111) are used and the time duration proportion of V1 and V2 depends on which vector is closer to V_{ref}. Fig.20 shows the relationship between the neutral point overvoltage and the modulation index and the location of the V_{ref}. Three locations have been considered, i.e., V_{ref} is aligned with V1 ($t_{(100)} = 0$), V_{ref} is aligned with V0 ($t_{(110)} = 0$) and V_{ref} is the middle between V0 and V1. Here, only the positive voltage overshoot is counted and as can be seen, when $t_{(110)} = 0$, meaning only V1 (100) is used, the voltage overshoot is higher because the CM voltage directly jumps from $-1/6V_{\text{dc}}$ (V1 (100)) to $+1/2V_{\text{dc}}$ (V7 (111)).

Fig.21 shows the impact of switching frequency on the neutral point voltage with a modulation index of 0.1. As seen, with the switching increasing from 10kHz to 100kHz, at 35kHz and 70kHz, the overvoltage is higher due to the switching frequency related harmonics coincide with the anti-resonant frequency (70kHz) of the motor. At even higher frequencies of 100kHz and 150kHz, the overvoltage reduces, which is likely due to the fact that the high-frequency harmonics are filtered by the parasitic elements of the electric machine.

Also, the modulation index affects the motor neutral overvoltage. With 70kHz switching frequency (anti-resonant frequency), Fig.22 shows the variation of the neutral overvoltage with modulation index. As seen, at very low modulation indices, the overvoltage is high due to higher chances of CM voltage reaching $+V_{\text{dc}}/2$ and $-V_{\text{dc}}/2$. The overvoltage reaches peak (70V) at the modulation index of 0.3, which is due to the double pulsing effect, where the CM voltage pulses are more closely spaced. At higher modulation indices, due to more steps in the CM voltage and the less chances of reaching $+V_{\text{dc}}/2$ and $-V_{\text{dc}}/2$ (more $+V_{\text{dc}}/6$ and $-V_{\text{dc}}/6$ instead), the overall CM voltage excitation is less, hence lower neutral point overvoltage.

It should be noted that the motor neutral overvoltage can occur even without cable.

IV. IMPACT OF WBG DRIVES ON MOTOR BEARINGS

As mentioned, the two main concerns related to motor overvoltages are the winding insulation premature failure due to partial discharge and motor bearing degradation

due to increased bearing current under high-switching speed, high switching frequency and associated motor neutral overvoltage. In this section, the motor bearing current has been investigated under various operating conditions. Fig. 23 shows the schematic diagram of the CM voltage/current path in the inverter-cable-motor system [18]. In Fig.23, v_{cm} is the CM voltage from the inverter. Z_0 represents the cable and motor CM impedance. v_{ng} is the motor neutral point voltage with reference to the ground as have been investigated in previous sections. Z_b is the bearing impedance and v_b is the bearing voltage. i_b is the bearing current. n, r, g represents the stator neutral, rotor and ground, respectively. C_{wr}, C_{rs} and C_{ws} are the stator winding to rotor, rotor to stator (ground) and winding to stator (ground) capacitances. Here, lumped elements are used to represent the parasitic capacitance, which in fact should be in the form of distributed elements. As can be seen, higher motor neutral voltage (v_{ng}) means higher bearing voltage (v_b) and potentially higher bearing current (i_b). It can also be seen that the bearing voltage waveform is not merely a direct proportion of the motor neutral point voltage, which indicates the distributed parasitic elements should be taken into account for the modelling rather than the simple lumped model shown in Fig.23.

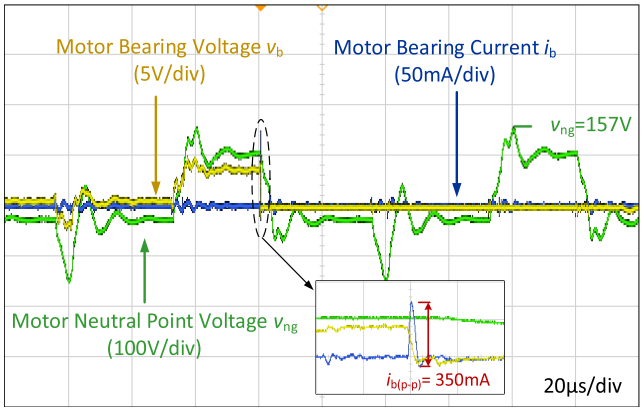

FIGURE 25. Motor bearing EDM current: dc-link voltage=200V, switching frequency=10kHz and motor speed=150rpm.

Fig.24 shows the motor neutral point voltage v_{ng}, motor bearing voltage v_b and motor bearing current i_b. Three modulation indices of 0.9, 0.5, 0.1 and three vector locations have been tested ($t_{(100)} = 0$, $t_{(110)} = 0$ and $t_{(100)} = t_{(110)}$). This provides a good representation of the scenarios with various modulation indices and vector locations. The test is carried out with the GaN inverter at the dc-link voltage of 200V, switching frequency of 10kHz and motor speed of 150rpm. As seen, there are clear *dv/dt* induced current $i_{b(p-p)}$ during the change of bearing voltage. There are also clear oscillations in the bearing current. The bearing voltage waveform has certain correlations with the motor neutral point voltage (including the overshoot), but the features are not exactly the same. It can be noted that during the neutral point voltage overshoot, the oscillation in the bearing current increases. At a lower modulation index, the motor neutral voltage overshoot increases, the reason of which has been explained in the previous section. Also, when there is only one active vector is used (i.e., either 110 or 100), the neutral voltage overshoot increases as well. These *dv/dt* driven bearing currents and the oscillation current observed may lead to accelerated bearing degradation.

Fig.25 shows the EDM type bearing current observed. The EDM current magnitude (350mA) is much higher than that of the *dv/dt* type of current. This high current magnitude is more harmful to the bearing. Also, when the EDM current occurs, the bearing voltage drops to zero as seen in Fig.25.

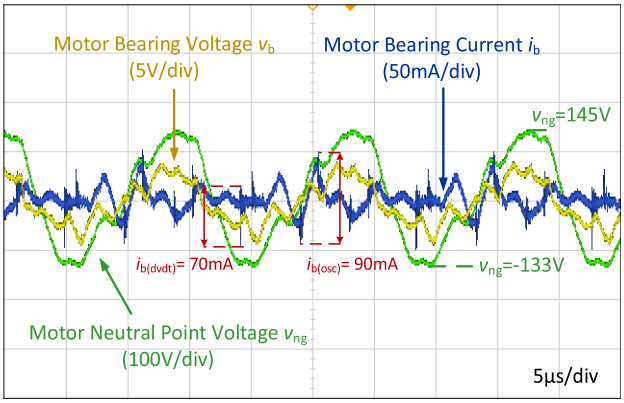

(a) Motor bearing *dv/dt* current and oscillating current

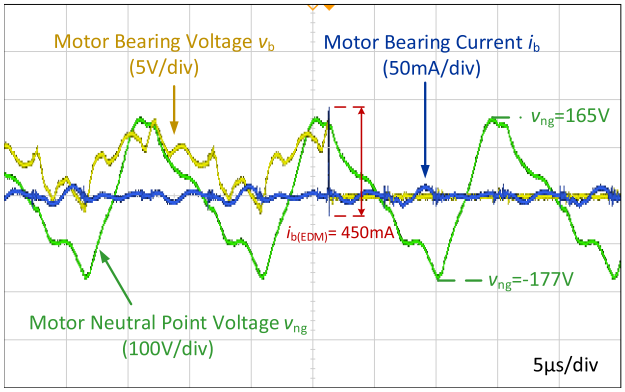

(b) Motor bearing EDM current

FIGURE 26. Motor bearing current with the inverter switching frequency of 70kHz and dc-link voltage of 200V.

Fig.26 further shows the bearing current when the switching frequency coincides with the motor CM anti-resonant frequency. As seen in Fig.26 (a), the magnitude of the oscillation current becomes slightly higher and the RMS value of the bearing current increases because the oscillation current ($i_{b(osc)}$) exists throughout the switching period. Fig.26 (b) shows the EDM bearing current.

V. CONCLUSION

In this paper, the impact of high switching speed and high switching frequency of WBG motor drives on electric machines has been revealed. The three types of motor

overvoltage, i.e., CM and DM motor terminal overvoltage and CM motor neutral overvoltage have been analyzed from both the time domain using the wave reflection theory and the frequency domain using the impedance (anti-resonant frequency) based method. It has been found that with very fast switching speed (tens of ns), the cable critical length that resulting in motor terminal voltage doubling are only several meters. The double pulsing effect makes the overvoltage even higher than double. The motor neutral overvoltage does not rely on the cable length and it will occur even without a cable, e.g., in an integrated inverter/motor system, which should be paid attention when designing the insulation system. The motor terminal overvoltage or motor neutral overvoltage becomes significantly higher (several times of the inverter output voltage) if the inverter switching frequency or its multiples coincides with the cable or electric machine anti-resonant frequency, which have been experimentally demonstrated in this paper. When using long cables or electric machines with a relatively low (tens of kHz) anti-resonant frequency, this issue should be paid special attention when the switching frequency of WBG inverters are also high. The direct reliability concerns due to the overvoltage investigated in this paper are on the motor winding insulation and bearing degradation or failure. The motor terminal overvoltage mainly drops on the first several turns of the coil/phase winding close to the terminal and the motor neutral overvoltage mainly drops on the last several turns of the coil/phase winding close to the neutral point. The insulation at these places of the winding should be paid special attention or strengthened. The increased level of bearing currents (*dv/dt*, oscillating and EMD currents) may accelerate the bearing degradation and should also paid special attention. The higher switching frequency of WBG motor drives means there will be more overvoltage events within certain period, putting more stress on the motor winding insulation and the bearing. Compared with conventional Si IGBT based drives with slower switching speed (*dv/dt*) and lower switching frequency, WBG motor drives makes the overvoltage more severe and there is a higher chance of the switching frequency or its multiples coincide with the anti-resonant frequency of the cable and electric machine. The future work will assess existing measures for mitigating motor overvoltages, including the filter-based approaches and active approaches such as using multilevel converters, soft-switching, quasi-multilevel modulation, advanced modulation with mitigation of DM or CM overvoltage. More efficient solutions will also be devised, e.g., selecting more optimized switching speed and switching frequency based on the whole system configuration and model, to achieve a holistic optimization of WBG motor drive systems.

REFERENCES

[1] P. Yi, P. K. S. Murthy, and L. Wei, "Performance evaluation of SiC MOSFETs with long power cable and induction motor," in *Proc. IEEE Energy Convers. Congr. Expo. (ECCE)*, Sep. 2016, pp. 1–7.

[2] S. Tiwari, O.-M. Midtgard, and T. M. Undeland, "SiC MOSFETs for future motor drive applications," in *Proc. 18th Eur. Conf. Power Electron. Appl. (EPE ECCE Eur.)*, Sep. 2016, pp. 1–10.

[3] B. Anirudh Acharya and V. John, "Design of output dv/dt filter for motor drives," in *Proc. 5th Int. Conf. Ind. Inf. Syst.*, Jul. 2010, pp. 562–567.

[4] M. J. Scott, J. Brockman, B. Hu, L. Fu, L. Xu, J. Wang, and R. D. Zamora, "Reflected wave phenomenon in motor drive systems using wide bandgap devices," in *Proc. IEEE Workshop Wide Bandgap Power Devices Appl.*, Oct. 2014, pp. 164–168.

[5] B. Narayanasamy, A. S. Sathyanarayanan, A. Deshpande, and F. Luo, "Impact of cable and motor loads on wide bandgap device switching and reflected wave phenomenon in motor drives," in *Proc. IEEE Appl. Power Electron. Conf. Expo. (APEC)*, Mar. 2017, pp. 931–937.

[6] W. Zhou, M. S. Diab, and X. Yuan, "Impact of parasitics and load current on the switching transient time and motor terminal overvoltage in SiC-based drives," in *Proc. IEEE Energy Convers. Congr. Expo. (ECCE)*, Oct. 2020, pp. 225–232.

[7] S. Sundeep, J. B. Wang, A. Griffo, and F. Alvarez-Gonzalez, "Anti-resonance phenomenon and peak voltage stress within PWM inverter fed stator winding," *IEEE Trans. Ind. Electron.*, early access, Jan. 8, 2021, doi: 10.1109/TIE.2020.3048286.

[8] B. Mirafzal, G. L. Skibinski, and R. M. Tallam, "A failure mode for PWM inverter-fed AC motors due to the antiresonance phenomenon," *IEEE Trans. Ind. Appl.*, vol. 45, no. 5, pp. 1697–1705, Oct. 2009.

[9] J. L. Guardado and K. J. Cornick, "The effect of coil parameters on the distribution of steep-fronted surges in machine windings," *IEEE Trans. Energy Convers.*, vol. 7, no. 3, pp. 552–559, Sep. 1992.

[10] *Motors and Generators*, Nat. Elect. Manuf. Assoc., NEMA Standards Publication MG1-2006, Apr. 2006.

[11] H. Xiong, J. Zhang, and A. Von Jouanne, "Control of variable frequency drive PWM to mitigate motor overvoltage due to double pulsing in reflected wave phenomenon," in *Proc. IEEE Energy Convers. Congr. Expo. (ECCE)*, Sep. 2018, pp. 6563–6570.

[12] M. S. Diab and X. Yuan, "A quasi-three-level PWM scheme to combat motor overvoltage in SiC-based single-phase drives," *IEEE Trans. Power Electron.*, vol. 35, no. 12, pp. 12639–12645, Dec. 2020.

[13] W. Zhou, M. S. Diab, and X. Yuan, "Mitigation of motor overvoltage in SiC-device-based drives using a soft-switching inverter," in *Proc. IEEE Energy Convers. Congr. Expo. (ECCE)*, Oct. 2020, pp. 662–669.

[14] R. M. Tallam and D. Leggate, "Control of a PWM voltage-source inverter in the pulse-dropping region to reduce reflected-wave motor overvoltage," *IEEE Trans. Ind. Appl.*, vol. 49, no. 2, pp. 873–879, Mar. 2013.

[15] M. S. Diab and X. Yuan, "A quasi-three-level modulation scheme to combat motor overvoltage in SiC-based drives with open-end stator winding configurations," in *Proc. 46th Annu. Conf. IEEE Ind. Electron. Soc. (IECON)*, Oct. 2020, pp. 844–851.

[16] X. Yuan, I. Laird, and S. Walder, "Opportunities, challenges, and potential solutions in the application of fast-switching SiC power devices and converters," *IEEE Trans. Power Electron.*, vol. 36, no. 4, pp. 3925–3945, Apr. 2021.

[17] W. Yin, "Failure mechanism of winding insulations in inverter-fed motors," *IEEE Elect. Insul. Mag.*, vol. 13, no. 6, pp. 18–23, Nov. 1997.

[18] Y. Xu, Y. Liang, X. Yuan, X. Wu, and Y. Li, "Experimental assessment of high frequency bearing currents in an induction motor driven by a SiC inverter," *IEEE Access*, vol. 9, pp. 40540–40549, 2021.

[19] J. He, G. Y. Sizov, P. Zhang, and N. A. O. Demerdash, "A review of mitigation methods for overvoltage in long-cable-fed PWM AC drives," in *Proc. IEEE Energy Convers. Congr. Expo.*, Sep. 2011, pp. 2160–2166.

[20] S. Narasimhan, S. Tewari, E. Severson, R. Baranwal, and N. Mohan, "Mitigation of common-mode noise in wide band gap device based motor drives," in *Proc. IEEE Appl. Power Electron. Conf. Expo. (APEC)*, Mar. 2016, pp. 2043–2050.

[21] A. von Jouanne, P. Enjeti, and W. Gray, "Application issues for PWM adjustable speed AC motor drives," *IEEE Ind. Appl. Mag.*, vol. 2, no. 5, pp. 10–18, Sep. 1996.

[22] Z. Liu and G. L. Skibinski, "Method to reduce overvoltage on AC motor insulation from inverters with ultra-long cable," in *Proc. IEEE Int. Electric Mach. Drives Conf. (IEMDC)*, May 2017, pp. 1–8.

[23] R. J. Kerkman, D. Leggate, and G. L. Skibinski, "Interaction of drive modulation and cable parameters on AC motor transients," *IEEE Trans. Ind. Appl.*, vol. 33, no. 3, pp. 722–731, May/Jun. 1997.

[24] A. von Jouanne and P. Enjeti, "Design considerations for an inverter output filter to mitigate the effects of long motor leads in ASD applications," in *Proc. Appl. Power Electron. Conf. (APEC)*, 1996, pp. 579–585.

[25] A. F. Moreira, T. A. Lipo, G. Venkataramanan, and S. Bernet, "High-frequency modeling for cable and induction motor overvoltage studies in long cable drives," *IEEE Trans. Ind. Appl.*, vol. 38, no. 5, pp. 1297–1306, Sep. 2002.
[26] V. Madonna, P. Giangrande, W. Zhao, H. Zhang, C. Gerada, and M. Galea, "On the design of partial discharge-free low voltage electrical machines," in *Proc. IEEE Int. Electr. Mach. Drives Conf. (IEMDC)*, May 2019, pp. 1837–1842.
[27] M. Diab and X. Yuan, "A modular quasi-multilevel converter using 10kV SiC MOSFETs for medium-voltage cable-fed variable-speed motor drives," in *Proc. IEEE ECCEAsia Conf.*, May 2021, pp. 1–6.

YIPU XU was born in Ningxia, China, in 1993. He received the B.Sc. degree in electrical engineering from the China University of Mining and Technology, Xuzhou, China, in 2016, where he is currently pursuing the Ph.D. degree with the School of Electrical and Power Engineering.

His current research interests include wide-bandgap devices and the impact of high-frequency drives on electric motor.

XIBO YUAN (Senior Member, IEEE) received the B.S. degree from the China University of Mining and Technology, Xuzhou, China, in 2005, and the Ph.D. degree from Tsinghua University, Beijing, China, in 2010, both in electrical engineering.

Since 2017, he has been a Professor with the Electrical Energy Management Group, Department of Electrical and Electronic Engineering, University of Bristol, Bristol, U.K., where he became a Lecturer, a Senior Lecturer, and a Reader, in 2011, 2015, and 2016, respectively. His research interests include power electronics and motor drives, wind power generation, multilevel converters, application of wide-bandgap devices, electric vehicles, and more electric aircraft technologies.

Prof. Yuan is a Fellow of IET. He is an Executive Committee Member of the U.K. National Centre for Power Electronics and the IET Power Electronics, Machines and Drives (PEMD) Network. He received the Isao Takahashi Power Electronics Award, in 2018. He holds the Royal Academy of Engineering/the Safran Chair in advanced aircraft power generation systems. He is an Associate Editor of IEEE TRANSACTIONS ON INDUSTRY APPLICATIONS and IEEE JOURNAL OF EMERGING AND SELECTED TOPICS IN POWER ELECTRONICS.

FEI YE was born in Anhui, China, in 1995. He received the B.Sc. degree in electrical engineering from Chaohu University, Anhui, in 2017. He is currently pursuing the M.Sc. degree with the School of Electrical and Power Engineering, China University of Mining and Technology.

His current research interests include power electronics and application of GaN HEMTs.

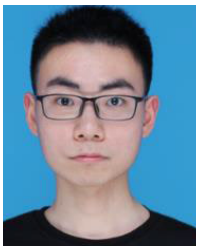

ZIHAO WANG was born in Henan, China, in 1998. He received the B.Sc. degree in electrical engineering from Zhejiang Sci-Tech University, Hangzhou, China, in 2019. He is currently pursuing the M.Sc. degree with the School of Electrical and Power Engineering, China University of Mining and Technology.

His current research interests include wide-bandgap devices and multilevel inverter.

YONGLEI ZHANG was born in Henan, China, in 1990. He received the B.Sc. degree from Henan Polytechnic University, Jiaozuo, China, in 2011, and the Ph.D. degree from the China University of Mining and Technology, Xuzhou, China, in 2018, both in electrical engineering.

Since 2018, he has been a Research Associate with the School of Electrical and Power Engineering, China University of Mining and Technology. He was a Visiting Scholar with the Electrical Energy Management Group, Department of Electrical and Electronics Engineering, University of Bristol, Bristol, U.K. His research interests include multilevel converters, parallel converters, wind power generation, and model predictive control.

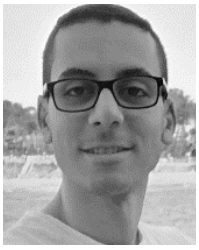

MOHAMED DIAB (Senior Member, IEEE) received the B.Sc. (Hons.) and M.Sc. degrees from Alexandria University, Egypt, in 2012 and 2015, respectively, and the Ph.D. degree from the University of Strathclyde, Glasgow, U.K., in 2019, all in electrical engineering.

He is currently a Research Associate with the Electrical Energy Management Group (EEMG), Department of Electrical and Electronic Engineering, University of Bristol, U.K. He is also an Assistant Lecturer with the Department of Electrical Engineering, Alexandria University. His main research interests include applications of wide-bandgap devices, electric motor drives, high-power electronic converters, and renewable energy conversion systems.

WENZHI ZHOU (Graduate Student Member, IEEE) received the B.Sc. degree from Dalian Jiaotong University, Dalian, China, in 2013, and the M.Sc. degree from Zhejiang University, Hangzhou, China, in 2016, both in electrical engineering. He is current pursuing the Ph.D. degree with the Electrical Energy Management Group, Department of Electrical and Electronic Engineering, University of Bristol, Bristol, U.K.

His research interests include wide-bandgap device applications, soft-switching, and partial discharge and motor drives.